Available online at www.eccomasproceedia.org
Eccomas Proceedia COMPDYN (2021) 3671-3684

ECCOMAS
Proceedia

COMPDYN 2021
8th ECCOMAS Thematic Conference on
Computational Methods in Structural Dynamics and Earthquake Engineering
M. Papadrakakis, M. Fragiadakis (eds.)
Streamed from Athens, Greece, 28 - 30 June 2021

KINEMATIC PILE-HEAD BENDING UNDER LARGE EARTHQUAKE-INDUCED SHEAR STRAINS

Stefano Stacul[1], Emmanouil Rovithis[2] and Raffaele Di Laora[3]

[1] Università di Pisa, Pisa, Italy
stefano.stacul@ing.unipi.it

[2] Institute of Engineering Seismology and Earthquake Engineering, ITSAK – EPPO
Thessaloniki, Greece
rovithis@itsak.gr

[3] Università degli Studi della Campania "Luigi Vanvitelli"
Aversa, Italy
raffaele.dilaora@unicampania.it

Abstract

The problem of kinematic bending moments imposed at the head of a single pile during the passage of seismic waves is explored under large shear strains in the surrounding soil. To this end, non-linear soil response at free-field conditions is derived numerically by a freely-available 1D code and then utilized to calibrate the constitutive law of soil introduced in a rigorous 3D Finite-Difference (FD) model of the soil-pile system employed to obtain pile's head bending moments. The pile is considered embedded to a normally-consolidated clay and seven earthquake records with different amplitude and frequency content are imposed as in-put motions at the base of the soil layer, thus allowing the investigation of pile kinematic bending with increasing levels of shear strains in the soil, exceeding the limit of equivalent-linear soil behavior. The performance of a simple analytical expression for predicting the kinematic bending moment at the pile-head is compared to the rigorous FD solution. It is concluded that this simple solution is still applicable, with slight modifications, for high shear strains related to non-linear soil behavior close to shear failure, provided that the proper mobilized soil properties from 1D soil response analysis are introduced.

Keywords: soil-pile interaction, 3D Finite-Difference, soil response, kinematic pile bending.

ISSN:2623-3347
Peer-review under responsibility of the organizing committee of COMPDYN 2021.
doi: 10.7712/120121.8738.19487

1 INTRODUCTION

Piles in earthquake-prone areas are traditionally designed to withstand inertial forces and moments coming from the oscillation of the superstructure. However, during the passage of seismic waves in the soil, an additional loading source is generated due kinematic interaction between pile and soil, which forces the pile to deform along its whole length, thus imposing additional bending on the pile. In some cases, this kinematic bending induced at the pile-head or at deeper elevations close to interfaces of soil layers with sharp stiffness contrast may be larger than pile bending due to inertial forces. Empirical evidence on this critical aspect of pile bending has been provided by post-earthquake observations in non-liquefiable soils [1–3]. The above field surveys recognized pile failures at depths where inertial forces from the superstructure are negligible. Thus, a reliable prediction of pile-head kinematic bending should follow a proper modelling of soil behavior at free-field conditions to estimate the deformation demand which the soil tries to impose on the pile.

To this end, the Equivalent Linear (EL) method is widely employed to derive free-field soil response when shear strains in the soil do not exceed a threshold value being around 0.2% [4]. In this case, soil response is far from failure and the EL approximation allows a reliable prediction of soil response by considering soil stiffness degradation and hysteretic damping increase with increasing strain. Under these conditions and upon considering for example a continuously inhomogeneous soil, a simplified analytical expression that is available in the literature [5] may be employed to assess kinematic pile-head bending moments by utilizing the mobilized stiffness of the soil which is compatible to the induced shear strains in free-field conditions.

On the other hand, under larger shear strains that may be generated when a soft soil is subjected to strong earthquake shaking, the assumption of soil response being controlled only by soil stiffness is no longer appropriate, since the shear strength of the soil plays a dominant role and, therefore, soil response cannot be captured by considering its stiffness degradation alone [6]. In this case, free-field ground response may be derived by a pertinent 1D analysis with a freely-available software like DEEPSOIL [7] once soil stiffness and strength properties are known. On the contrary, the prediction of pile kinematic bending under large shear strains in the soil seems to be possible only by numerical analyses of complex soil-pile models with advanced constitutive laws at least for the soil.

Upon considering that such type of analyses are excessively demanding for pile design practice, this paper explores the applicability of the abovementioned analytical formula by properly adapting its input parameters in the presence of shear strains close to soil failure. For this reason, a series of Finite-Difference (FD) analyses are performed by employing experimentally validated constitutive models for the case of a normally-consolidated clay. Rigorous analyses results in terms of kinematic pile-head bending are compared with the predictions of a proposed analytical expression including frequency effects.

2 SOIL-PILE SYSTEM UNDER STUDY

The system under investigation refers to a single fixed-head pile embedded in a 30m thick soil layer resting on a rigid base (Figure 1). The pile is a linear elastic cylindrical solid beam of diameter d = 1 m, length L = 20 m, Poisson's ratio ν_p = 0.15, unit weight ρ_p = 24 kN/m^3 and elastic modulus E_p = 25 GPa. A soft normally-consolidated clay layer is considered the low-strain stiffness and strength properties of which are described in the ensuing.

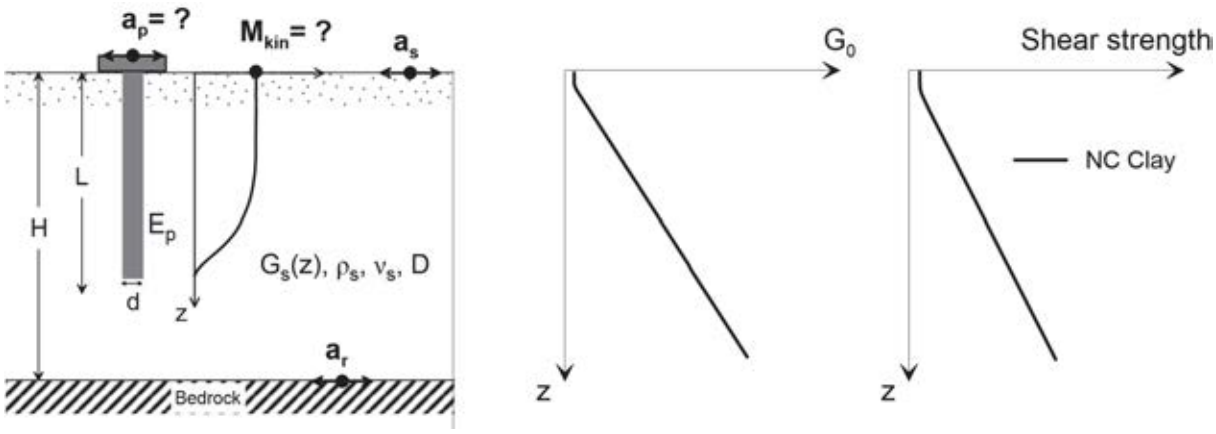

Figure 1: Single elastic fixed-head pile in a normally-consolidated (NC) clay soil.

2.1 Normally-consolidated (NC) Clay properties

A fine-grained, fully saturated normally-consolidated (NC) clay having a unit weight γ_{sat} = 17.9 kN/m^3 and a plasticity index I_p = 40% is considered. The ratio s_u / σ'_{v0} of the undrained shear strength (s_u) over the vertical effective geostatic stress for a NC clay can be derived by [8]:

$$\frac{s_u}{\sigma'_{v0}} = 0.11 + 0.0037 I_p \tag{1}$$

with I_p expressed in percentage. For I_p = 40% the above expression yields:

$$s_u(kPa) = 2.1z \tag{2}$$

where z is the depth from the ground surface. Upon considering that the low-strain shear modulus G_0 is proportional to depth through a multiplier of the associated shear strength profile (i.e. $G_0 = 800 s_u$) the following distribution of G_0 with depth is obtained:

$$G_0(MPa) = 1.7z \tag{3}$$

which corresponds to a shear wave propagation velocity profile in the form:

$$V_{s0} = 30z^{0.5} \tag{4}$$

and a $V_{s,30}$ value at 100 m/s, referring to soil type D according to EC8. The above expression was also adopted by Travasarou and Gazetas [9] to describe the V_{s0} profile of a particularly soft normally consolidated clay in a real site. The above low-strain stiffness and the strength profiles are plotted in Figure 1.

2.2 Input motions

A set of seven earthquake recordings selected from the PEER Strong Motion Database [10] were imposed at the base of the soil layer, in the form of vertically propagating SH waves, to investigate pile-head kinematic bending under seismic loading. The selected records were acquired from stations resting on soil type A or B of the USGS classification system. The 5%-damped acceleration response spectra of the selected motions normalized by the peak rock acceleration (PRA) are plotted in Figure 2. Three levels of increasing intensity of the input motion were examined by scaling the records to three levels of Peak Rock Acceleration (PRA) considered at 0.10g, 0.15g and 0.25g.

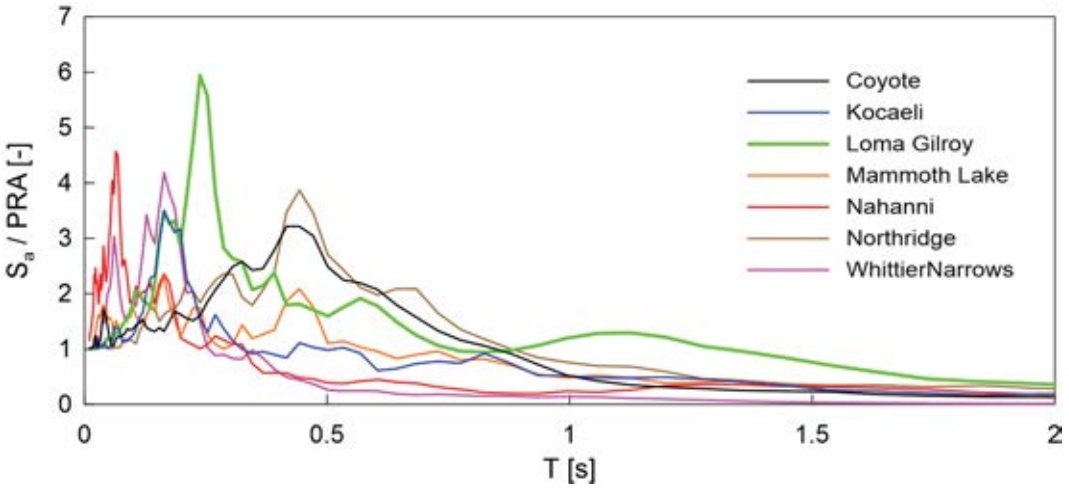

Figure 2: Normalized elastic response acceleration spectra of the selected input motions.

3 NUMERICAL ANALYSES

First, a one-dimensional free-field soil response analysis was performed with the DEEPSOIL code [7], by considering equivalent linear (EL) and non-linear (NL) soil behaviour. The Finite-Difference (FD) code FLAC3D [11] was then employed to perform non-linear time history analyses by implementing a rigorous 3D model of the soil-pile system with pertinent constitutive models to describe soil behaviour.

3.1 DEEPSOIL non-linear soil model

The General Quadratic/Hyperbolic (GQ/H) model [12] was adopted to model the backbone curve of the shear stress-strain relationship for the non-linear (NL) analyses in time domain performed with DEEPSOIL. The GQ/H model allows the shear strength of the soil to be directly introduced as an input parameter, contrary to the Modified Kondner Zelasko (MKZ) model [13], which may overestimate the shear strength of the soil depending on the values of the curve-fitting parameters [14]. For the hysteretic soil behaviour during unloading and reloading, the associated stress-strain loops were defined on the basis of the non-Masing Modulus Reduction and Damping with reduction Factor (MRDF) formulation proposed in Phillips and Hashash [15], to avoid damping overestimation at large shear strains when Masing rules are adopted [16].

3.2 FLAC3D soil-pile model

Following a sensitivity analysis on critical modelling aspects such as model size, discretization scheme, pile and pile-soil interface, the final 3D FD soil – pile model (Figure 3) implemented in FLAC3D code, has a base, width, and height equal to 30m, 30m, and 31m, respectively. The one-meter-thick bottom layer models the elastic bedrock with a shear wave velocity at 800 m/s and the same unit weight like the soil layers above. The grid-element size in the vertical direction (z-axis) was selected according to the indications provided in Kuhlemeyer and Lysmer [17]. The first 20 m were discretized with 80 layers of 0.25 m thickness each, while 20 layers of 0.50 m thickness each were adopted to discretize the soil profile between 20 and 30 m.

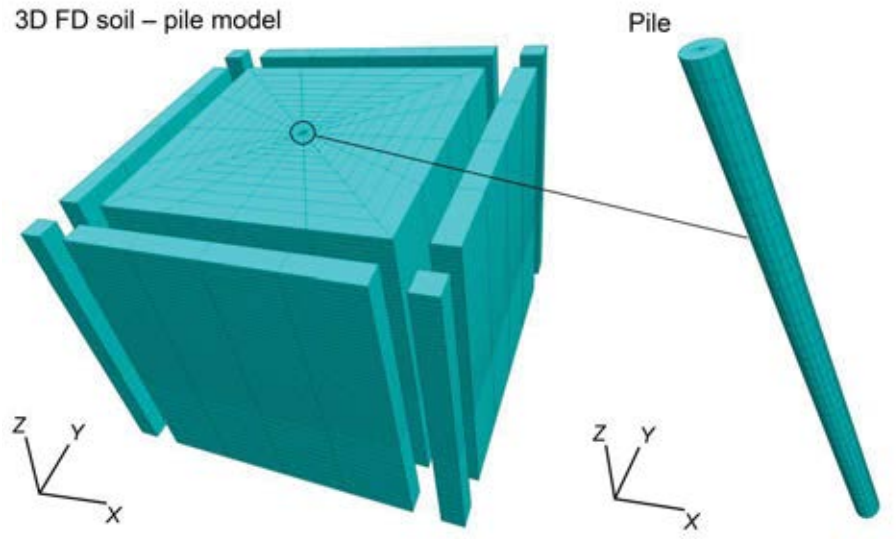

Figure 3: 3D Finite-Difference (FD) soil – pile model employed in FLAC3D code.

The same discretization was adopted in the DEEPSOIL code, satisfying the criterion of a frequency $f_{max,i}$ ($= V_{s0,i} / 4H_i$), that a layer of thickness Hi and shear wave velocity $V_{s0,i}$ can propagate, above 25 Hz [7]. A linear elastic behavior of the pile material and a bonded connection between soil and pile elements were assumed. The latter was based on the fact that soil-pile contact stresses under kinematic loading are negligible compared to those induced by forces or moments applied at the pile-head [18].

Nonlinear soil response in dynamic analyses was accounted for by means of the UCSDCLAY model [19]. The UCSDCLAY model is a pressure-independent 3D elasto-plastic material model, which enables reproducing nonlinear hysteric shear behavior, and it allows the shear strength of the soil to be introduced as a direct input. Rayleigh damping, which is commonly applied to take into account small strain (viscous) damping or to remove high frequency noise, was found to be unnecessary.

3.3 UCSDClay model calibration

A recursive calibration procedure was followed to obtain similar non-linear behavior between the GQ/H and USCDClay models. In this regard, the following steps were performed: (Figure 4): (i) first, the GQ/H model was calibrated by the Vucetic and Dobry [20] curves for I_p = 40% (noted in Figure 4 as "DS fit.1"), (ii) the fitted DEEPSOIL curves were employed to calibrate the USCD Clay model introduced in FLAC3D and (iii) the fitted FLAC3D-based curves were employed to calibrate again the GQ/H model (noted in Figure 4 as "DS fit.2"). In this manner, it was possible to derive comparable $\tau - \gamma$ backbone curves between the two models (Figure 4c) at the expense of higher hysteretic damping at large strains with respect to the experimental data (Figure 4b).

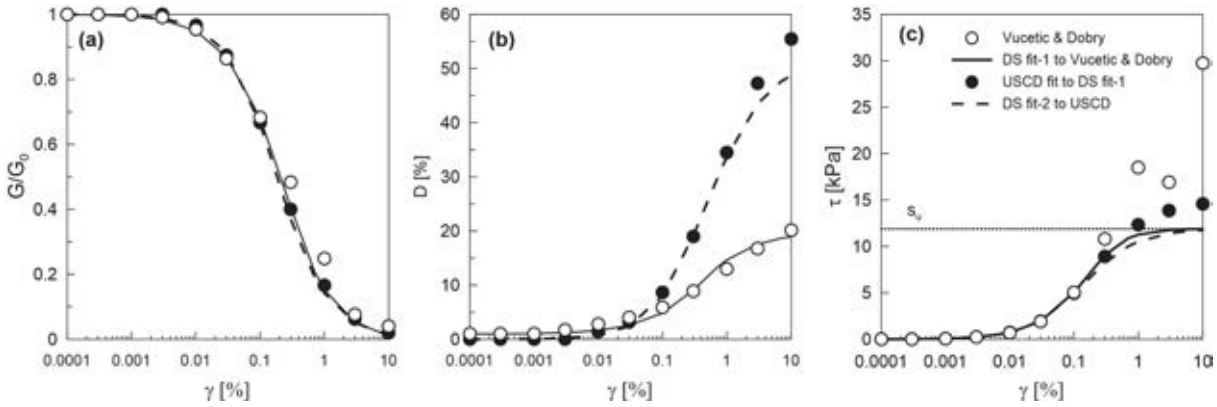

Figure 4: Calibration of DEEPSOIL and FLAC3D soil models for the NC Clay case based on Vucetic and Dobry [20] G/G0 – γ – D(%) curves for Ip = 40% regarding: (a) Stiffness degradation, (b) Hysteretic damping increase and (c) Shear stress-strain backbone curve at the depth of 4.375m (the implied shear strength derived in DEEPSOIL is also mentioned).

4 SOIL RESPONSE AT FREE-FIELD CONDITIONS

Non-linear analyses results of the free-field ground response derived with DEEPSOIL code under the prescribed input motions is shown in Figure 5, in terms of peak ground acceleration (Figure 5a), maximum shear strain (Figure 5b) and maximum shear stress (Figure 5c) profiles, referring to average values between those computed separately for each one of the seven base excitations. An effective shear strain profile was then computed as 0.65 times the maximum strain developed at any depth and was then employed to obtain the corresponding mobilized shear modulus and damping profiles based on the calibrated $G/G_0 - \gamma - D(\%)$ curves. In this manner, a single mobilized stiffness and damping profile was derived for each one of the seven input motions. An average mobilized G profile obtained by averaging these seven profiles is shown in Figure 5d. All the results shown in Figure 5 correspond to the maximum PRA at 0.25g. The same analyses results obtained with DEEPSOIL by implementing this time the Equivalent Linear (LE) approximation to model soil behavior are also plotted in Figure 5. In this case, a frequency independent expression [i.e. $G^* = G(1+2iD)$] was adopted for the complex formulation of the shear modulus while the effective shear strain ratio was set at 0.65. The degradation of the shear modulus and the increase of the hysteretic damping of the soil with increasing shear strain were modeled by implementing the $G/G_0 - \gamma - D(\%)$ curves proposed in Vucetic and Dobry [20] for the plasticity index under consideration (I_p = 40%). It is noted that for the first 1.5 m of the soft NC clay profile, the low-strain shear modulus (G_0) and the undrained shear strength (s_u) were considered constant at 2.55 MPa and 6.2 kPa, respectively, due to a numerical issue observed in DEEPSOIL when very low values of the above parameters are introduced. Below 1.5m, the s_u and the G_0 profiles follow the linear variation with depth described by Equations 2 and 3, respectively.

It is observed that under the EL assumption, a sudden increase of the peak ground acceleration is observed close to the ground surface, being in qualitative agreement with analytical elasto-dynamic investigations reported in Rovithis et al. [21] for a similar shear wave velocity profile. On the contrary, when the non-linear behavior of soil is modeled by the rigorous GQ/H model, ground acceleration is de-amplified as it propagates through the soil due to the low shear strength of the soft clay, which limits the transmission of shear stresses. Such a behavior has also been reported in experimental studies of the seismic behavior of soft clays [22]. This indicates that the EL approximation is not able to capture the complex soil behavior, which is also reflected in the τ-γ loops derived at two depths close to the ground surface (Figure 6) for PRA = 0.25g. The strong non-linear behavior of the soil generates large inelastic

strains on the order of 1%, while the developed shear stresses are bounded by the low shear strength s_u of the soft clay. Apparently, the above soil response cannot be reproduced by the linear elastic τ-γ relationship under the EL assumption (Figure 6). This does not mean absence of energy dissipation through the hysteretic behavior of the soil, as the latter is taken into account through the complex shear modulus during each iteration of an EL analysis.

The corresponding average profiles of free-field ground response obtained with FLAC3D are also plotted in Figure 5. The agreement between DEEPSOIL NL and FLAC3D analysis indicates that critical trends of ground response may be reproduced in a similar manner, which provides confidence that the adopted model in FLAC3D is able to reproduce highly non-linear ground response and, therefore, kinematic soil-pile interaction over a wide range of shear strains.

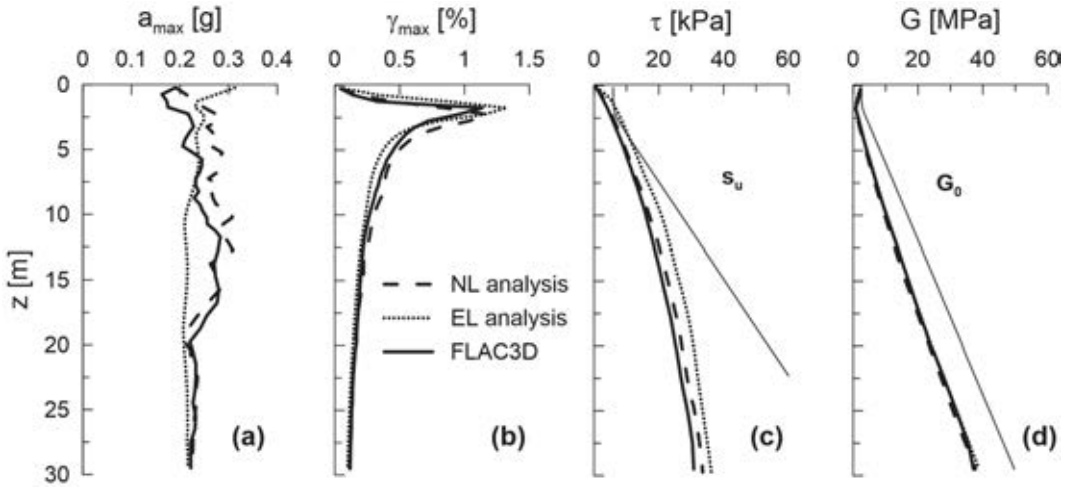

Figure 5: Comparison of free-field ground response analysis results between DEEPSOIL (EL and NL analysis) and FLAC3D for the NC clay profile in terms of: (a) PGA profile (b) average maximum shear strain profile (c) average shear stress and (d) mobilized shear modulus G with depth. All plots refer to PRA = 0.25g.

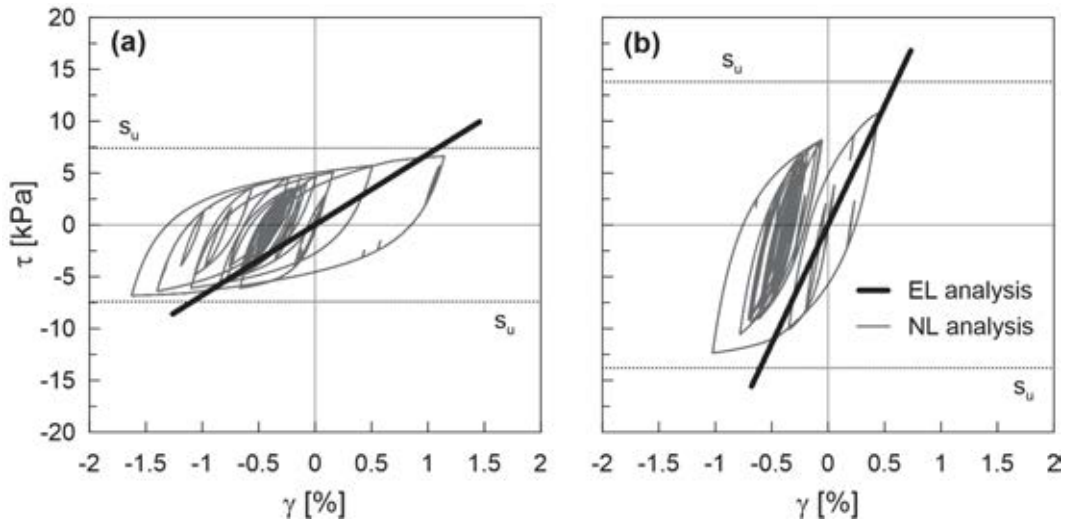

Figure 6: Comparison of EL and NL soil response analysis with DEEPSOIL for the NC clay profile in terms of τ - γ loops at the depth of: (a) 2.625 m and (b) 5.125 m. All plots refer to PRA = 0.25g.

5 PILE-HEAD KINEMATIC BENDING

In the general case of an inhomogeneous soil profile with shear stiffness varying continuously with depth according to the law:

$$G_s(z) = G_{sd}\left[a + (1-a)\frac{z}{d}\right]^n \tag{5}$$

where $G_s(z)$ is the depth-varying soil shear modulus, G_{sd} is the shear modulus at the depth of one pile diameter (i.e., at $z = d$) and a, n are dimensionless factors controlling the stiffness profile, the active length (L_a) of the pile may be calculated by the expression [5, 23, 24]:

$$L_a = \frac{d}{1-a}\left\{\left[a^{\frac{n+4}{4}} + \frac{5}{16}(n+4)(1-a)\left(\frac{\pi}{2}\frac{E_p}{E_{sd}}\right)^{\frac{1}{4}}\right]^{\frac{4}{n+4}} - a\right\} \tag{6}$$

where E_{sd} is the Young's modulus of elasticity of the soil at one pile diameter depth.

5.1 Constant ground acceleration

Upon considering that there is an effective portion of the soil controlling pile-head bending, which is proportional to a characteristic wavelength of the soil-pile system, Di Laora and Rovithis [5] introduced the notion of an effective soil curvature [$(1/R)_{s,eff}$] as the ratio of the shear strain $\gamma_s(z_{eff})$ at an effective depth z_{eff} over z_{eff} [i.e. $(1/R)_{s,eff} = \gamma_s(z_{eff}) / z_{eff}$] to derive a simple analytical expression for the kinematic bending moment at the head of a pile in a continuously inhomogeneous soil, such as that described by Equation 5, and proved that under constant ground acceleration, a_s, the ratio of the pile-head curvature $(1/R)_p$ over $(1/R)_{s,eff}$ for long piles is equal to 1, which allows calculation of pile-head kinematic bending by the formula:

$$M_{kin} = E_p I_p (1/R)_p = E_p I_p (1/R)_{s,eff} = E_p I_p \frac{\gamma_s(z_{eff})}{z_{eff}} \tag{7}$$

where the depth z_{eff} is considered as one half of the pile's active length L_a:

$$z_{eff} = \frac{L_a}{2} \tag{8}$$

The equilibrium of a 1D soil column with constant mass density ρ_s and variable shear modulus $G(z)$ with depth yields that in static conditions $\gamma(z_{eff})$ may be expressed as:

$$\gamma_s(z_{eff}) = \frac{a_s \rho_s z_{eff}}{G_s(z_{eff})} \tag{9}$$

where $G(z_{eff})$ is the mobilized shear modulus of the soil at z_{eff}. Thus, Equation 7 may be rewritten as:

$$M_{kin} = E_p I_p \frac{a_s \rho_s}{G_s(z_{eff})} \tag{10}$$

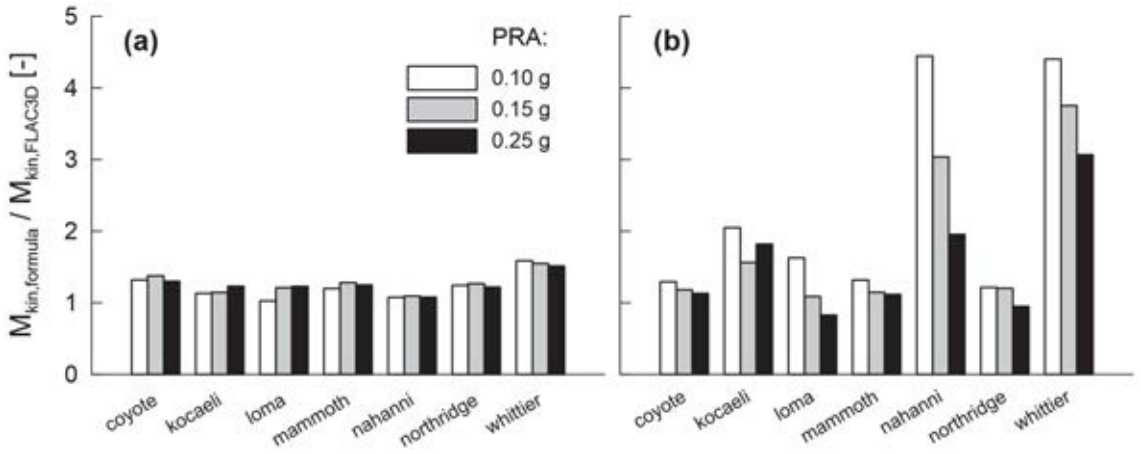

Figure 7: Ratios of kinematic pile-head bending moment between 3D FD analyses (FLAC3D) and the predictions of (a) Equation 7 and (b) Equation 10.

In order to apply the above formulae, one has fit the mobilized shear modulus profile derived from 1D ground response analysis, to the formula of $G_s(z)$ in Equation 5 in order to obtain the parameters G_{sd}, a and n and then calculate La and z_{eff} from Equations 6 and 8, respectively. As the above parameters are interrelated, an iterative procedure may be followed by considering the value of $L_a = 10d$ as a starting point and employing a least square linear (i.e. $n = 1$) fit. A single iteration leads to quite accurate results.

The performance of Equations 7 and 10 is compared to the rigorous 3D Finite-Difference model response in Figure 7, in the form of ($M_{kin,formula}$ / $M_{kin,FLAC3D}$) ratio for all the examined input motions scaled to 0.10g, 0.15g and 0.25g. Each group of bars refers to a different base excitation noted in the abscissa of the plots. To this end, the maximum shear strain $\gamma_{max,s}(z_{eff})$ at z_{eff} was introduced in Equation 7, while the peak ground acceleration at soil surface was employed to derive $M_{kin,formula}$ in Equation 10. Both of these parameters were obtained by the FLAC3D analyses for the purpose of this comparison.

It is observed that for the particularly soft NC Clay under consideration, where the maximum shear strain at z_{eff} attains considerably large values up to 0.8 - 1 % (Figure 5b), the kinematic pile-head bending predicted by Equation 7 is much closer to the rigorous FD solution (Figure 7a), denoting that the maximum shear strain at z_{eff} is a better indicator of the developed pile-head bending compared to the peak ground acceleration at surface (Figure 7b), when soil behavior is close to failure (Figure 5c). However, despite its better performance, Equation 7 may still be quite conservative for certain base excitations, like in the case of the Whittier base motion where an overestimation of 50% is attained.

5.2 Frequency effects: Proposed analytical expression

The above over-prediction of kinematic bending is explainable, though, as it follows the original conservative assumption of constant ground acceleration to derive Equation 7, implying low-frequency excitations. This is valid if the frequency content of the time variant parameter $\gamma_s(z_{eff})$ controlling the kinematic demand is low enough to be considered as almost statically applied. Otherwise, the bending moment attains lower values as the shear strain (and the corresponding effective soil curvature) is a decreasing function of the excitation frequency regardless of the soil properties [5].

In this case, frequency effects in kinematic bending may be accounted for by implementing the expression of the dynamic $(1/R)_{p,dyn}$ over the static $(1/R)_{p,static}$ pile curvature ratio proposed in Di Laora and Rovithis [5]:

$$\frac{(1/R)_{p,dyn.}}{(1/R)_{p,static}} = \left[1 + 0.02a_{eff,La}^3\right]^{-1} \tag{11}$$

In the above expression, $a_{\mathrm{eff,La}}$ is a dimensionless frequency which controls the kinematic response of the pile in the dynamic regime [5, 24]:

$$a_{eff,La} = \frac{\omega L_a}{V_{s,av}} \tag{12}$$

where ω is the cyclic frequency of the excitation, L_a is the active length of the pile (Equation 6) and $V_{\mathrm{s,av}}$ refers to an average shear wave velocity along z_{eff} given by:

$$V_{s,av} = V_{s,d}\frac{L_a(a-1)(n-2)}{4d}\left[\left(a+(1-a)\frac{L_a}{d}\right)^{1-n/2} - a^{1-n/2}\right]^{-1} \tag{13}$$

where V_{sd} is the mobilized shear wave at one pile diameter depth which may be derived by the corresponding value of G_{sd} once the mobilized shear modulus profile is fitted to a linear function as mentioned above.

Obviously, Equation 11 is a continuous function of ω. In order to obtain a single-valued prediction of the kinematic pile-head moments in the dynamic regime, a mean cyclic frequency $\omega_{\mathrm{m},\gamma}$ is considered as an index of the frequency content of the shear strain time history at z_{eff}. Following the definition of the mean period (T_m) of an acceleration time history introduced in Rathje et al. [25], $\omega_{\mathrm{m},\gamma}$ may be computed from:

$$\omega_{m,\gamma} = 2\pi\frac{\sum_i c_{i,\gamma}^2}{\sum_i c_{i,\gamma}^2\left(\frac{1}{f_i}\right)} \tag{14}$$

where $C_{\mathrm{i},\gamma}$ refer to the Fourier amplitudes of the shear strain time history at z_{eff} and f_i are the discrete Fourier transform frequencies between 0.25 Hz and 20 Hz. In this manner, a mean dimensionless frequency $a_{\mathrm{eff,m,La}}$ of the shear strain demand at z_{eff} may be defined by introducing $\omega_{\mathrm{m},\gamma}$ in Equation 12:

$$a_{eff,m,La} = \frac{\omega_{m,\gamma} L_a}{V_{s,av}} \tag{15}$$

Upon introducing $a_{\mathrm{eff,m,La}}$ in Equation 11, a single value of the $(1/R)_{\mathrm{p,dyn}}$ / $(1/R)_{\mathrm{p,static}}$ ratio may be computed for each base excitation according to the associated value of $a_{\mathrm{eff,m,La}}$. Taking also into account that for long piles $(1/R)_{\mathrm{p,static}} = (1/R)_{\mathrm{s,eff}}$, the kinematic pile-head bending moment including frequency effects may be derived by the expression:

$$M_{kin} = E_p I_p \frac{\gamma_{\max,s}(z_{eff})}{z_{eff}}\left[1 + 0.02a_{eff,m,La}^3\right]^{-1} \tag{16}$$

The performance of the above expression against the rigorous FD solution is compared in Figure 8. The improvement of the agreement between the two solutions with respect to that shown in Figure 7a cannot be overstated, denoting maximum deviations of less than 10%.

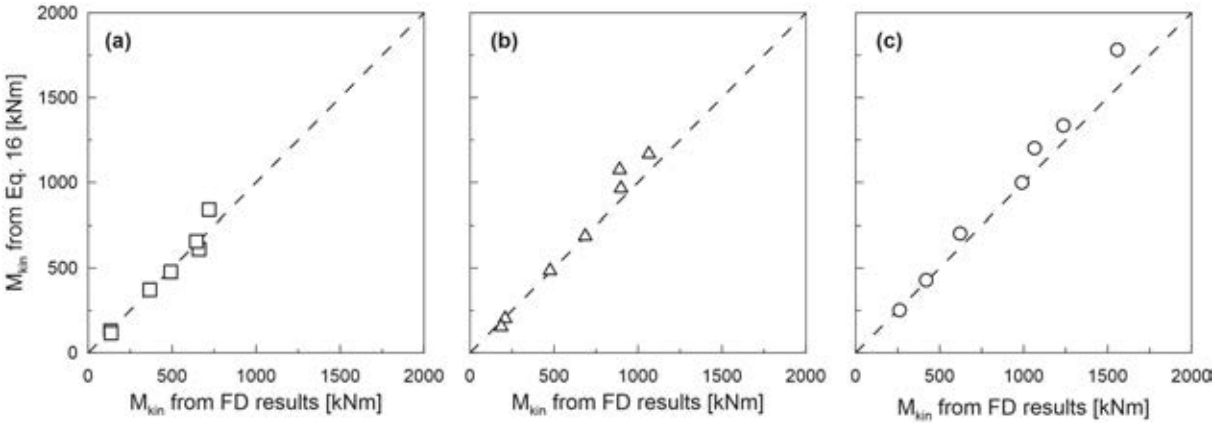

Figure 8: Comparison of kinematic pile-head bending moments between Equation 16 and FD results for PRA at (a) 0.10g (b) 0.15g and (c) 0.25g. Each point in the plots refers to a different input motion.

This suggests that the simple analytical formula in Equation 16 is applicable even in the highly nonlinear range of soil response close to failure, provided that the associated shear strain demand induced by the surrounding soil and the corresponding mobilized stiffness profile are introduced. It may thus be asserted that dynamic effects result in modifying solely soil deformations at free-field conditions while soil-pile kinematic interaction mechanism remains static. The latter was first discussed by Di Laora et al. [26] for homogeneous soils and confirmed further in Di Laora and Rovithis [5] for nonhomogeneous soils. The results of this study extend, therefore, the validity of the simple analytical solutions to the non-linear range of soil response, denoting that kinematic soil-pile interaction is controlled by the soil stiffness even if the response of the soil is controlled by its strength. The above finding generalizes earlier indications [27–30] of the controlling role of the mobilized soil stiffness on pile kinematic bending.

6 CONCLUSIONS

Kinematic pile-head bending moments were explored under increasing earthquake-induced shear strains in the soil, by means of a rigorous 3D Finite Difference model of the soil-pile system, taking into account both stiffness degradation and strength of the soil. The numerical results were compared to the predictions of a proposed simple formula properly adapted for the non-linear regime of soil response over an earlier publication of the Authors. The main conclusions can be summarized as follows:

- While in the linear and static regime Equations 7 and 10 return identical predictions of pile-head bending moments, in the non-linear regime the use of ground surface acceleration is no longer reliable and the maximum shear strain at an effective depth equal to one half of the pile's active length becomes the dominant soil response parameter controlling kinematic bending at the pile-head.
- The simplified formula in Equation 16 may be employed to derive kinematic pile-head bending in the non-linear dynamic range of soil response. In this regard, a 1D free-field non-linear soil response analysis, which properly considers both stiffness degradation and soil strength, should be performed to derive the necessary input parameters in the formula.
- A mean cyclic frequency was suggested (Equation 14) as a single index of the frequency content of the shear strain time history at one half of the pile's active length. Such an in-

terpretation of the frequency content of a shear strain time history has not been previously explored in the kinematic bending of piles.

- It was proven that dynamic and non-linear effects result in modifying solely soil deformations at free-field conditions, while soil-pile kinematic interaction mechanism remains static and linear. This shed lights to the actual nature of kinematic soil-pile interaction mechanism which may be considered as stiffness-controlled even if free-field soil response is strength-controlled.

ACKNOWLEDGEMENTS

The authors wish to thank ITASCA for a loan of software within the Itasca Education Partnership (IEP).

REFERENCES

[1] T. Tazoh, K. Shimizu, T. Wakahara, Seismic Observations and Analysis of Grouped Piles. *Dynamic Response of Pile Foundations—Experiment, Analysis and Observation*, ASCE, Geotechnical Special Publication, **11**, 1-20, 1987.

[2] H. Mizuno, Pile damage during earthquake in Japan. T. Nogami, editor. *Dynamic Response of Pile Foundations*, ASCE, Geotechnical Special Publication, **11**, 53-78, 1987.

[3] S. Nikolaou, G. Mylonakis, G. Gazetas, T. Tazoh, Kinematic pile bending during earthquakes: analysis and field measurements. *Géotechnique*, **51**(5), 425-440, 2001.

[4] J. Kaklamanos, B.A. Bradley, E.M. Thompson, L.G. Baise, Critical parameters affecting bias and variability in site‐response analyses using KiK‐net downhole array data. *Bulletin of the Seismological Society of America*, **103**(3), 1733-1749, 2013.

[5] R. Di Laora, E. Rovithis, Kinematic bending of fixed-head piles in nonhomogeneous soil. *Journal of Geotechnical and Geoenvironmental Engineering*, **141**(4), 04014126, 2015.

[6] J. Shi, D. Asimaki, From stiffness to strength: Formulation and validation of a hybrid hyperbolic nonlinear soil model for site‐response analyses. *Bulletin of the Seismological Society of America*, **107**(3), 1336-1355, 2017.

[7] Y.M.A. Hashash, M.I. Musgrove, J.A. Harmon, D.R. Groholski, C.A. Phillips, D. Park, *DEEPSOIL 6.1, User Manual*. Urbana, IL, Board of Trustees of University of Illinois at Urbana-Champaign, 2016.

[8] A.W. Skempton, Discussion: Further data on the c/p ratio in normally consolidated clays. *Proceedings of the Institution of Civil Engineers*, **7**, 305-307, 1957.

[9] T. Travasarou, G. Gazetas, On the linear seismic response of soils with modulus varying as a power of depth: the Maliakos marine clay. *Soils and Foundations*, **44**(5), 85-93, 2004.

[10] T. Ancheta, R. Darragh, J.P. Stewart, E. Seyhan, W. Silva, B. Chiou, K. Wooddell, R. Graves, A. Kottke, D. Boore, T. Kishida, J. Donahue, *PEER NGA-West2 Database*,

PEER Report 2013/03 Pacific Earthquake Engineering Research Center Headquarters at the University of California, Berkeley, 2013.

[11] Itasca, Fast Lagrangian Analysis of Continua (FLAC3D 6.00). Itasca Consulting Group Inc, Minneapolis, USA, 2017.

[12] D. R. Groholski, Y.M.A. Hashash, M. Musgrove, J. Harmon, B. Kim, Evaluation of 1-D Non-linear site response analysis using a general quadratic/hyperbolic strength-controlled constitutive model. *Proceedings of the 6th International Conference on Earthquake Geotechnical Engineering*, Christchurch, New Zealand, 2015.

[13] N. Matasovic, *Seismic response of composite horizontally-layered soil deposits*. Ph.D. Thesis, University of California, Los Angeles, 1993.

[14] D.R. Groholski, Y.M.A. Hashash, B. Kim, M. Musgrove, J: Harmon, J.P. Stewart, Simplified model for small-strain nonlinearity and strength in 1D seismic response analysis. *Journal of Geotechnical and Geoenviromental Engineering*, **142**(9): 04016042, 2016.

[15] C. Phillips, Y.M.A. Hashash, Damping formulation for non-linear 1D site response analyses. *Soil Dynamics and Earthquake Engineering*, **29**, 1143-1158, 2009.

[16] A.O. Kwok, J.P. Stewart, Y.M. Hashash, N. Matasovic, R. Pyke, Z. Wang, Z. Yang, Use of exact solutions of wave propagation problems to guide implementation of non-linear seismic ground response analysis procedures. *Journal of Geotechnical and Geoenvironmental Engineering*, **133**(11), 1385-1398, 2007.

[17] R.L. Kuhlemeyer, J. Lysmer, Finite element method accuracy for wave propagation problems. *Journal of the Soil Dynamics Division*, **99**, 421-427, 1973.

[18] R. Di Laora, G. Mylonakis, A. Mandolini, Size limitations for piles in seismic regions. *Earthquake Spectra*, **33**(2), 729-756, 2017.

[19] A. Elgamal, L. Yan, Z. Yang, J.P. Conte, Three-dimensional seismic response of Humboldt Bay bridge foundation-ground System, *Journal of Structural Engineering*, ASCE, **134**(7), 1165-1176, 2008.

[20] M. Vucetic, R. Dobry, Effect of soil plasticity on cyclic response. *Journal of Geotechnical Engineering*, **17**, 89-107, 1991.

[21] E. Rovithis, C. Parashakis, G. Mylonakis, 1D harmonic response of layered inhomogeneous soil: Analytical investigation, *Soil Dynamics and Earthquake Engineering*, **31**, 879-890, 2011.

[22] T.K. Garala, G.S.P. Madabhushi, Seismic behaviour of soft clay and its influence on the response of friction pile foundations, *Bulletin of Earthquake Engineering*, **17**, 1919–1939, 2019.

[23] X. Karatzia, G. Mylonakis, Discussion of kinematic bending of fixed-head piles in non-homogeneous soil by Raffaele Di Laora and Emmanouil Rovithis, *Journal of Geotechnical and Geoenvironmental Engineering*, **142**(2), 07015042, 2016.

[24] M. Iovino, R. Di Laora, E. Rovithis, L. de Sanctis, The beneficial role of piles on the seismic loading of structures, *Earthquake Spectra*, **35**(3), 1141-1162, 2019.

[25] E.M. Rathje, N.A. Abrahamson, J.D. Bray, Simplified frequency contents estimates of earthquake ground motions. *Journal of Geotechnical and Geoenviromental Engineering*, **124**(2), 150-158, 1998.

[26] R. Di Laora, A. Mandolini, G. Mylonakis, Insight on kinematic bending of flexible piles in layered soil. *Soil Dynamics and Earthquake Engineering*, **43**, 309-322, 2012.

[27] M. Mucciacciaro, S. Sica, Nonlinear soil and pile behaviour on kinematic bending response of flexible piles. *Soil Dynamics and Earthquake Engineering*, **107**, 195-213, 2018.

[28] S. Stacul, A. Franceschi, N. Squeglia, Effect of non-linear soil response and pile post-cracking behavior on seismically induced bending moments in fixed-head long piles. In *7th International Conference on Earthquake Geotechnical Engineering* (ICEGE 2019), CRC Press/Balkema, Rome, Italy, June 17-20, 2019.

[29] S. Stacul, N. Squeglia, Simplified assessment of pile-head kinematic demand in layered soil. *Soil Dynamics and Earthquake Engineering*, **130**, 105975, 2020.

[30] T.K. Garala, G.S. Madabhushi, R. Di Laora, Experimental investigation of kinematic pile bending in layered soils using dynamic centrifuge modelling. *Géotechnique*, 1-16, 2020.